2013 IEEE/RSJ International Conference on Intelligent Robots and Systems (IROS)
November 3-7, 2013. Tokyo, Japan

Lift Generation of Hummingbird Wing Models with Flexible Loosened Membranes*

Hiroto Tanaka, Haruka Suzuki, Ikuo Kitamura, Masateru Maeda, and Hao Liu

Abstract— **Hummingbirds are promising reference for small flying robots in terms of their excellent ability to hover. Wing kinematics and shape of a hovering hummingbird were measured with four high-speed video cameras. Four types of wing models consisting of carbon fiber rods and polymer membranes with the same planform as the hummingbird wing were fabricated. 1-degree-of-freedom (DOF) flapping experiments with the wing models were performed, where the wing deformation and vertical force (hereafter called 'lift') were measured. The model wings demonstrated similar feathering deformation as that of the hummingbird in the upstroke. In addition, the model wing with a loosened membrane which caused larger feathering deformation produced lift enough to support the weight of the hummingbird. The results suggest that hovering hummingbirds could be modeled as a pair of 1-DOF flapping wings with a thin membrane which passively feathers.**

I. Introduction

Flapping flight of vertebrates or insects has attracted attention from a broad range of research fields including biology, aerospace engineering, or robotics, because of its potential for high efficiency and high agility such as hovering, rapid acceleration or rapid turn. Unsteady aerodynamics of flapping wings of small flyers in nature is well reviewed in [1]. From the viewpoint of robotics, one of the biggest challenges is to mechanically realize the wing kinematics under severely restricted mass. While the wing kinematics of vertebrates or insects is a combination of three degree of freedom (DOF) rotational motions, called flapping, feathering, and lead-lag (or elevating) [2], most of the previous flyable artificial flappers only have a 1-DOF flapping mechanism with flexible wing membranes [3-8] or flexible hinges at the wingbase [9, 10] which passively achieve feathering. Although two or more DOF active wing motions was used in some researches, the total weight of the mechanical flapper was heavier than the flying animals with the same wing size [11]. The combination of active flapping and passive feathering is an effective solution for ultra-lightweight small flying robots in terms of the simplicity of the mechanics which cuts down the mass for actuators, structures, or circuit boards. In addition, the flapping robots with the same mass as the flying animals or insects could be useful tools for study of flight biomechanics.

*This work was supported in part by Shanghai Jiao Tong University and Chiba University International Cooperative Research Center and MEXT KAKENHI Grant Number 24760197, 21360078, 18100002, and 4402-24-2412007.

H. Tanaka is with the Shanghai Jiao Tong University and Chiba University International Cooperative Research Center, Chiba University, Chiba, 263-8522 Japan (phone: +81-43-274-2945; fax: +81-43-274-2944; e-mail: htanaka@ chiba-u.jp).

H. Suzuki, I. Kitamura, M. Maeda, and Hao Liu are with the Graduate School of Engineering, Chiba University, Chiba, 263-8522 Japan.

In this paper, we focused on a hovering flight of a hummingbird aiming to realize the wing kinematic similar to that of the hummingbird with a combination of 1-DOF flapping and passive feathering in artificial flapping wings. Hummingbirds are well-known for their excellent ability to hover. In addition, they have several characters as a promising model for flapping robots: Their wingspan and mass is less than 150 mm and 10 g, respectively, which matches the size range of MAVs (Micro Air Vehicles) [12-14]. As for the wing structure, unlike the other birds of which wings fold at the elbow during upstroke, hummingbirds' wings do not fold both in upstroke and downstroke because the elbow joint is too close to the shoulder (wingbase) [15]. Hence their wing kinematics and aerodynamics are similar to hovering insects such as Dipteran rather than the other birds [16-20]. Since the length of the arm and hand of the hummingbirds is typically less than the half the wing length, passive deformation of the feathers may play an important role.

For this purpose, firstly we measured wing kinematics and shape of a real hummingbird in hovering flight. Based on the measurement, four types of model wings were created and tested. In particular, we employed a loosened wing membrane which allows larger deformation. The model wings showed similar tendency of feathering deformation as that of the hummingbird wing in upstroke. The model wing with the loosened membrane and a curved leading edge like the real wing produced lift enough to support the weight of the hummingbird.

II. Measurement of a Hovering Flight of a Hummingbird

A. High-speed video shooting and mass measurement

A hovering flight sequence of an Amazilia hummingbird (*Amazilia amazilia*) was recorded with four high-speed video cameras in a large conservatory (1140 m^2 in area and 16 m in ceiling height) in Tama Zoological Park (Tokyo, Japan) in November 2012. The environmental temperature was 22 °C and the wind speed was less than 0.0015 m s^{-1} which was measured with a hot-wire anemometer (Anemomaster Lite Model 6006, Kanomax Japan Inc., Japan). The high-speed video cameras we used were three FASTCAM SA3 (Photron Ltd., Japan) with resolution of 1024×1024 pixels and a FASTCAM SA2 (Photron Ltd., Japan) with resolution of 2048×1080 pixels. For all the cameras, the frame rate and exposure time were set at 2000 frames per second and 1/3000 seconds, respectively. The position and orientation of the hovering hummingbird was adjusted by setting a feeder of nectar which was hanged from a tree branch. To improve the contrast of the captured images, three white background boards were placed behind the feeder. On the assumption that the kinematics of the hovering hummingbird was bilaterally

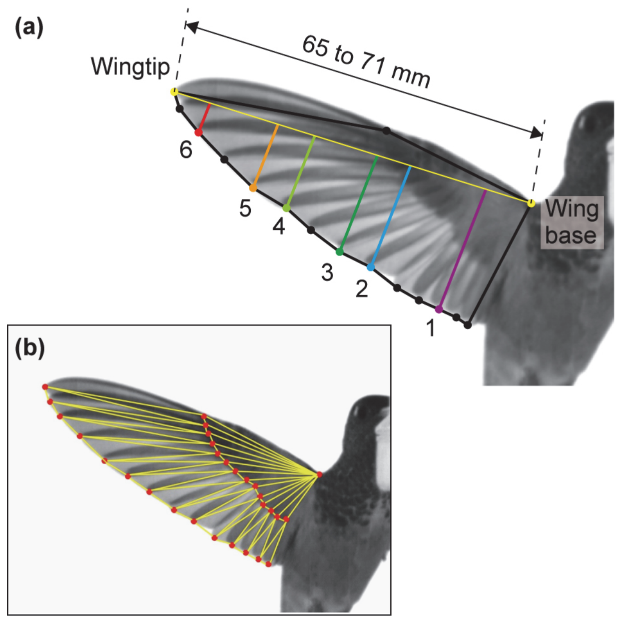

Figure 1. Tracking points for 3-D reconstruction of the right wing of a hummingbird. (a) Numbered lines represent measured chord lines. (b) Polygonal surfaces were used for estimation of wing area.

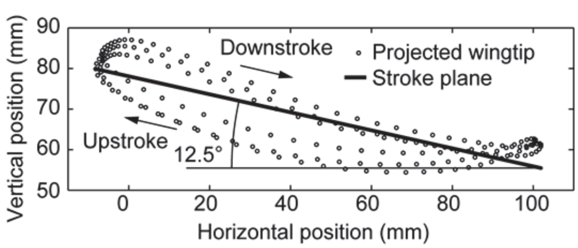

Figure 2. A stroke plane and a wing tip trajectory projected to the median sagittal plane of the hummingbird.

symmetric, we captured only the right wing in order to fully utilize the resolution.

Two days after the video shooting, the mass of the hummingbird was measured with a single-axis load cell, LTS-100GA, and a 12-bit AD interface, PCD-300A (Kyowa Electronic Instruments Co., Ltd, Japan), with sampling rate of 1000 Hz. A ring-shaped perch was attached to the load cell and located under the feeder of nectar. The hummingbird hovered to suck the nectar from the feeder and occasionally took a rest on the ring-shaped perch, and then the mass was measured. The average mass for the three events was around 5.4 g.

B. 3-D reconstruction of wing kinematics and shape

3-D coordinates of feature points of the wing were reconstructed by using more than two of four captured images with motion analysis software (Dipp-Motion Pro 3D, Ditect Co., Ltd., Japan). The cameras were calibrated using known eight points of a rigid framework. We manually tracked the wingbase, wingtip and tips of feather shafts of the right wing (figure 1 (b)). A time series of the obtained coordinate values was digitally smoothed by weighted moving-average method with a hamming window. Number of points for the moving average was 21 and cutoff frequency was set at 200 Hz which was higher than the flapping frequency of the measured

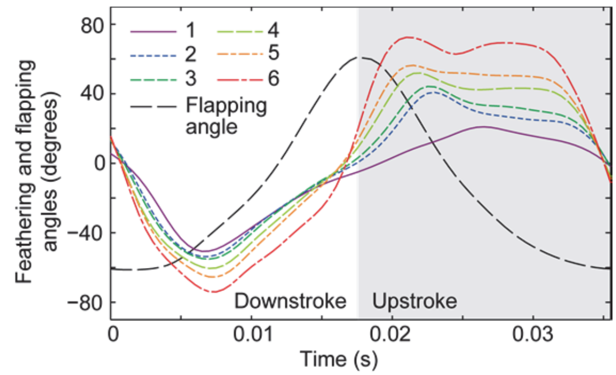

Figure 3. Time variation of feathering angle of the hummingbird wing. Each color corresponds to the wing chord in figure 1 (a).

TABLE I. FEATHEING DEFORMATION OF THE HUMMINGBIRD

Chord No.	Spanwise position (mm)	Min (degrees)	Max (degrees)	Amplitude (degrees)
1	10	-51	21	72
2	24	-54	41	95
3	30	-55	44	99
4	42	-61	52	113
5	49	-65	56	121
6	62	-74	72	146

humming bird, 29 Hz.

The wing outline was simplified into a polygonal line (shown as black lines in figure 1 (a)) as a design basis of the model wings. The detailed designs are described in Section III. A wing length (a distance between the wingbase and wingtip) varied during flapping cycles, ranging from 65 to 71 mm. Wing area was estimated by polygonal surfaces generated from the tracked points (figure 1 (b)). The variation of the estimated wing area in a single flapping cycle was around 20% of the maximum value.

A stroke plane is defined as follows. First, a trajectory of the wingtip for three flapping cycles was projected to a median sagittal plane of the hummingbird. Second, an approximate line of the projected points was calculated by least-square approach (figure 2). Finally, the stroke plane was defined as a plane which is perpendicular to the median sagittal plane and intersects the sagittal plane on the approximate line of the projected wingtip trajectory. A stroke plane angle, which was defined as an angle between the stroke plane and a horizontal plane, was 12.5°.

A flapping angle was defined as follows: First, the wingbase–wingtip line was projected to the stroke plane. Then, the flapping angle was defined as the angle between the projected line on the stroke plane and the median sagittal plane. A flapping amplitude, defined as a difference between the maximum and minimum flapping angles, was 110°.

Based on the observation that spanwise deformation of the hummingbird wing was not significant, wing chord lines were defined as perpendicular lines from the six trailing edge points, which are the tips of the feathers (marked 1 to 6 in figure 1 (a)), to the wingbase-wingtip line. Note that our definition of the chord does not include the leading edge

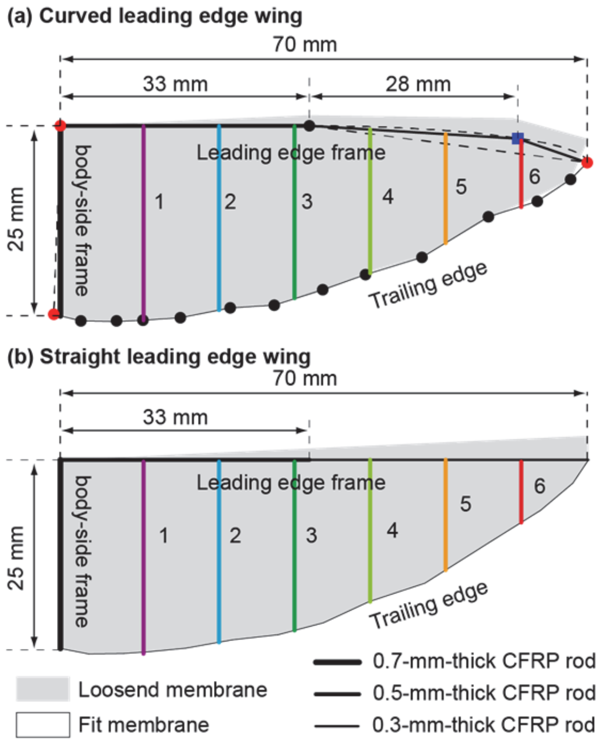

Figure 4. Design of the wing frames and membranes.

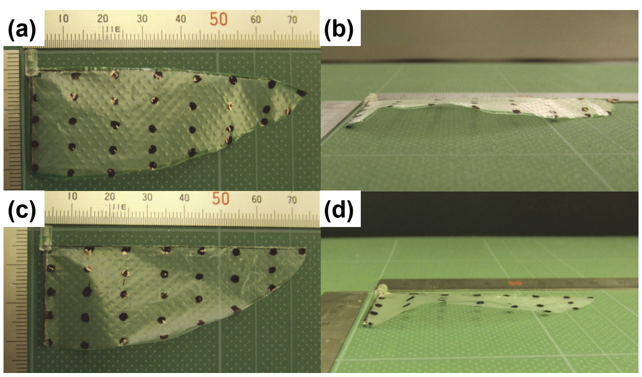

Figure 5. (a, b) A model wing with a curved leading edge and a loosened-membrane. (c, d) A model wing with a straight leading edge and a loosened-membrane wing (c, d). Black dots were painted as markers for motion analysis.

therefore is different from a conventional definition. Feathering angle was defined as an angle between the wing chord and the stroke plane.

Figure 3 shows feathering angles for the six chords in a single flapping cycle. The color of each line corresponds to the chord color in figure 1. The feathering angle increased as spanwise position of the chord moved from the wingbase to the wingtip, meaning that the wing surface twisted. The clear difference between the downstroke and the upstroke was observed in the feathering angle near the body (No. 1 in figure 3): The minimum feathering angle of the near-body chord (No.1) reached -50° in the downstroke, while the maximum angle was 21° in the upstroke. On the other hand, the minimum of the near-wingtip chord (No. 6) was -74° and the maximum was 72° (table I). It means that the twist of the wing surface in the upstroke was larger than that in the downstroke. One of possible reasons of this asymmetry of the wing twist was that a feathering rotation of the shoulder joint was musculoskeletally limited in upstroke.

TABLE II. SHAPE, SIZE AND MASS OF THE FABRICATED WINGS

Wing shape		Wing length (mm)	Wing area (mm^2)	Mass (g)
Leading edge	Membrane			
Curved	Loosened	70	1406	0.11
Curved	Fit	70	1313	0.13
Straight	Loosened	70	1406	0.10
Straight	Fit	70	1313	0.12

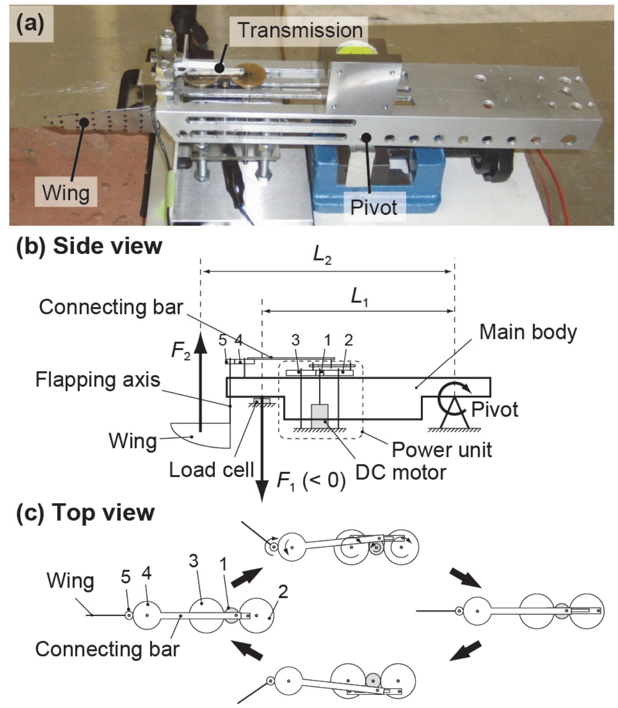

Figure 6. (a) 1-DOF flapping mechanism. (b) Side-view schematic of the lift measurement setup. (c) Top-view schematic of the transmission. Rotational gears are numbered from 1 to 5.

III. LIFT MEASUREMENT OF MODEL WINGS MIMICKING A HUMMINGBIRD

Wing feathers deform passively due to aerodynamic forces or inertia. Therefore the chordwise deformation and associated change in the feathering angles of the hummingbird wing described in Section II is also assumed to be passive. Based on this assumption, we fabricated four model wings and tested them with a 1-DOF flapping mechanism. Each wing model consists of a leading edge frame, a body-side frame and a flexible membrane. In particular, we employed a loosened membrane which allows larger feathering deformation and evaluated its effect on lift generation.

A. Design and fabrication of model wings

The leading edge and body-side frames were made of carbon fiber reinforced polymer (CFRP) rods. The wing surface membrane was made of a 20-µm-thick polyethylene film.

We designed two types of leading edge (LE) shapes: a curved LE (figure 4 (a)) and a straight LE (figure 4 (b)). The outline of the curved LE wing was determined by projecting the tracked points of the hummingbird wing when the wing area was maximum onto the plane which was determined by the wingbase, wingtip and near-body feather tip (red dots in figure 4 (a)). To mimic the curved leading edge of the outermost primary feather, an additional point (blue square marker near No.6 chord in figure 4 (a)) was set on a quarter ellipse which was drawn from the middle point on the leading edge to the wingtip.

The outline of the straight LE wing was generated by shifting the leading edge and trailing edge of the curved LE wing maintaining the chord length. Since straight leading edges are relatively easy to fabricate, this type of wings can be seen in many other researches of flapping flying robots and commercially available flying toys.

A "Fit-membrane" wing was created by attaching a membrane which has exactly the same planform as the wing planform (solid black line in figure 4). On the other hand, a "loosened-membrane" wing was fabricated by cutting out larger membrane than the wing planform and attaching it to the leading edge and body-side frames. That is, the wing surface made of the loosened membrane has extra flexibility compared to the "fit-membrane" model. The planar shapes of the expanded loosened membranes, which are shown in grey color in figure 4, were designed by rotating the leading edge of the fit membranes until the wing area matches the maximum wing area of the hummingbird which is illustrated as polygonal surfaces in figure 1 (b). The fit and loosened membranes were 1313 mm^2 and 1406 mm^2 in area for both curved and straight LE cases, respectively.

The fabricated wings with loosened membranes are shown in figure 5. The sizes and masses of the fabricated wings are summarized in table I. The variation of the mass is due to variation of the amount of glue used.

B. *Experimental setup for lift measurement*

Each fabricated wing was attached to a 1-DOF tethered flapping mechanism as shown in figure 6 (a). Rotational output of a DC motor (22V28, Portescap, USA) was converted to flapping motion via a transmission composed of gears and a slider (figure 6 (b, c)). The main body of the mechanism was supported by a pivot axis and a load cell. A power unit consisting of the transmission and the motor was separated from the main body in order to prevent vibration of the main body (figure 6 (b)). The power unit and the main body were loosely connected via a connecting bar. A DC power supply (U8002A, Agilent Technologies, USA) was used to apply constant voltage to the motor. The flapping amplitude was designed to be 110° and the flapping frequency was set at 28 Hz throughout the experiments, which are close to those of the measured hummingbird (110° and 29 Hz, respectively). Reynolds number was 5.1×10^3 where the reference velocity was wingbeat-cycle averaged speed of the middle of the wing, 4.1 m/s, and the reference length was the mean chord length, 19 mm.

As illustrated in figure 6 (b), the vertical component of the force generated by the wing (hereafter called 'lift'), F_2, was measured using a balance mechanism in which counter force, F_1, was measured with a single-axis load cell, LMA-A-5N, and a 12-bit AD interface, PCD-300A (Kyowa Electronic Instruments Co., Ltd, Japan), with sampling rate of 2000 Hz. The measured data was digitally smoothed with a lowpass filter of 120-Hz cut-off frequency using FFT and inverse FFT functions in MATLAB (MathWorks, USA).

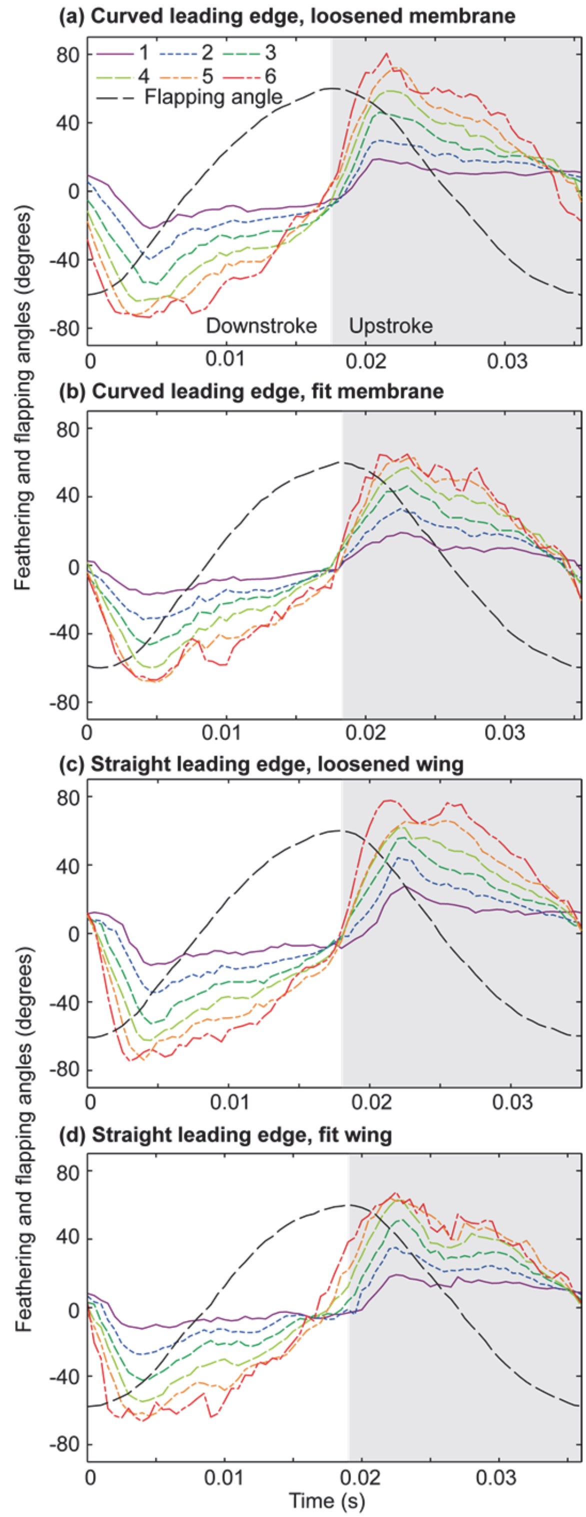

Figure 7. Time variation of the feathering angles in the model wings. Numbers and colors correspond to the wing chords in figure 4.

TABLE III. FEATHERING DEFORMATION OF THE MODEL WINGS

		Curved LE loosened wing			Curved LE fit wing			Straight LE loosened wing			Straight LE fit wing		
Chord No.	Spanwise position (mm)	Min (degrees)	Max (degrees)	Amp. (degrees)	Min (degrees)	Max (degrees)	Amp. (degrees)	Min (degrees)	Max (degrees)	Amp. (degrees)	Min (degrees)	Max (degrees)	Amp. (degrees)
1	11	-22	19	40	-17	19	36	-19	28	46	-12	19	32
2	21	-40	30	70	-32	33	65	-35	44	79	-27	35	62
3	31	-54	46	101	-46	46	93	-53	56	109	-42	51	94
4	41	-64	58	122	-60	57	117	-62	62	124	-55	63	118
5	51	-72	72	144	-68	63	131	-74	66	140	-63	64	128
6	61	-74	81	154	-67	65	132	-75	78	152	-66	68	134

Moments around the pivot joint due to the lift, F_2, and the counter force acting on the load cell, F_1 (< 0), balanced out as

$$F_1L_1 + F_2L_2 = 0 \quad (1)$$

where L_1 and L_2 are the lengths of the moment arms for the measured force, F_1, and lift, F_2, respectively. Since the actual location of the center of pressure on the wing is unknown, here we assumed that the center of pressure locates at the half the wing length. Then, lift, F_2, was calculated as

$$F_2 = - F_1L_1 / L_2 \quad (2)$$

In our experimental setup, L_1 and L_2 were 120 mm and 155 mm, respectively.

Wing shape during flapping was measured with three high-speed video cameras (FASTCAM SA3, Photron Ltd., Japan. 2000 frames per second, 1024 $\times$ 1024 pixels and exposure time of 1 / 3800 seconds). Multiple black markers were painted on the wing surface (figure 5 (a, c)). The 3-D coordinates of these markers were reconstructed with motion analysis software (Dipp-Motion Pro 3D, Ditect Co., Ltd., Japan).

Feathering angles of the six chord lines were measured, which are located at similar position to those of the hummingbird (figure 1 (a) and figure 4 (a, b)).

C. *Feathering deformation*

Time variation of the feathering angles of the curved LE loosened-membrane wing are shown in figure 7 (a), and the maximum, minimum and amplitude of each chord are shown in table III. Although the active wing motion was simple 1-DOF flapping, feathering deformation of the model wings demonstrated a similar tendency to that of a real hummingbird in the upstroke in that the wing surface twisted and the feathering angle increased as the spanwise position moved from the wingbase to the wingtip. The feathering in two consecutive strokes (downstroke and upstroke) of the model wings, however, was almost symmetric, while the hummingbird wing showed an asymmetry. In the real hummingbird case, there was less twist in the downstroke than in the upstroke. In other words, wing deformation in upstroke of the real hummingbird can be regarded as a simple1-DOF flapping with a flexible membrane.

D. *Effect of loosened membranes on wing deformation*

It was confirmed that the loosened membranes resulted in larger feathering deformation. In case of the curved leading edge wings, the loosened membrane showed larger feathering amplitude than that of the fit membranes by 4% to 17% (9% on average, table III). For the straight leading edge wings, the increase of the feathering amplitude ranged from 5% to 44%, (19% on average).

Even though the planform of the fit membrane matched the initial planform of the wing frames, deflection and torsion of the frames allows the fit membrane feathered. In fact, the fit-membrane wings also showed considerable feathering deformations (figure 7 (b, d)).

E. *Effect of leading edge curvature on wing deformation*

Curvature of the leading edge did not make clear difference in the feathering deformation. For the loosened-membrane cases, deviation in the feathering amplitude from those of the straight leading edge cases ranged from -13% to 2% (-5% on average) for the loosened-membrane cases, and -1% to 13% (3% on average) for the fit-membrane cases (table III).

F. *Lift and efficiency*

The wingbeat-cycle averaged lift for each wing is shown in figure 8 (a). Half the weight of the hummingbird described in Section II (2.7 g) is also displayed as a reference. Note that in our single-wing experiments there is no aerodynamic interaction between left and right wings, which could occur in hovering of real hummingbirds.

The curved leading edge loosened-membrane wing marked the highest average lift, 26.5 mN, which is equals to half the weight of the hummingbird, 26.5 mN (figure 8 (a)). It should be emphasized that this result suggests that flapping wing of hovering hummingbird could be modeled as a 1-DOF flapping wing with a conventional frames and membranes composition.

The lift of the curved loosened wing (26.5 mN) was 12% larger than that of the curved fit wing (23.7 mN). The lift of the straight loosened wing (23.1 mN) was also 12% larger than that of the straight fit wing (20.6 mN). These results demonstrate that loosened membranes could enhance lift of 1-DOF flapping wings with the same wing planform (original shape of the wing frames).

The curved loosened wing generated 15% higher lift (26.5 mN) than the straight loosened wing (23.1 mN). Also, the curved fit wing generated greater lift (23.7 mN) than the straight fit wing (20.6 mN). Considering the small difference of feathering amplitude between the two wings (table III), the difference of the lift could be not derived from feathering deformation but due to the aerodynamic effect of the leading edge shape.

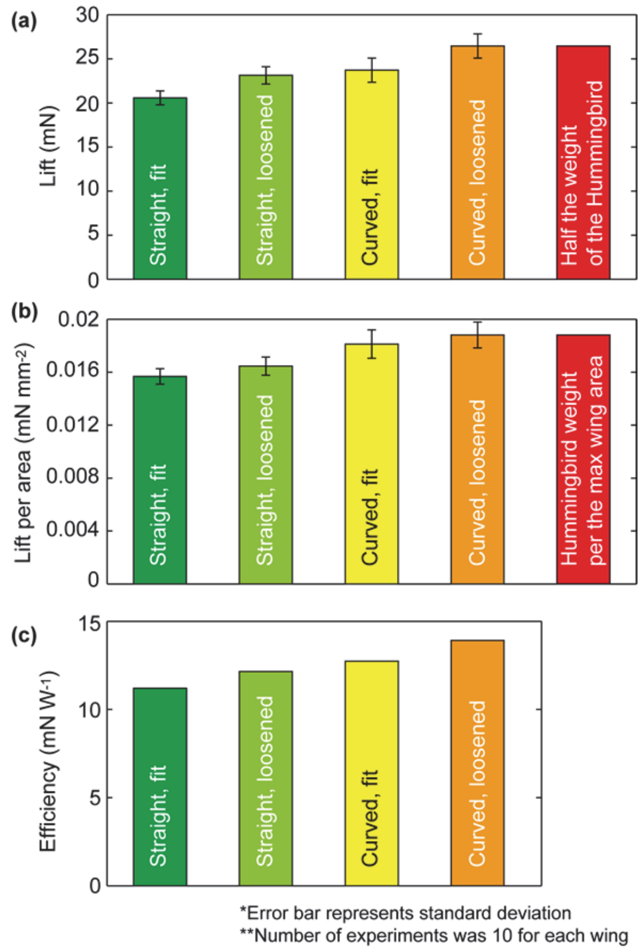

Figure 8. Average lift (a), average lift per wing area (b), and efficiency of lift generation (c). Lift of the hummingbird was calculated as the half the body mass. Input power was calculated from input constant voltage and average current.

To compensate the influence of the area of the membrane, we calculated "lift per area" values by dividing the lift values with the area of the membranes shown in table II. As a result, although the calculated values for the fit membranes and the loosened membranes were close to each other, the loosened-membrane wings still showed higher values than the fit-membrane wings (figure 8 (b)): The difference was less than 6%. Therefore, it can be said that loosened membranes are simply useful to extend the wing area for increase of lift.

Finally, we calculated lift per input power as a reference index of efficiency (figure 8 (c)). Input power was approximated by multiplying the applied constant voltage and displayed current value of the DC supply. No fluctuation in the current values was observed. As shown in table IV, the wings with the loosened membranes required higher input power than those with the fit membranes in both leading edge cases. The efficiency of the wings with the loosened membranes, however, were higher than those with the fit membranes due to the larger lift values (figure 8 (a, c)). Consequently, the wing with the curved leading edge and the loosened membrane achieved the highest lift and efficiency among the wing models tested in this paper.

TABLE IV. APPLIED VOLTAGE, DISPLYAED CURRENT, AND EFFICIENCY

Wing shape	Voltage (V)	Current (A)	Power (W)	Efficiency ($mN\ W^{-1}$)
curved, loosened	10.0	0.190	1.90	13.9
curved, fit	10.0	0.186	1.86	12.7
straight, loosened	10.0	0.190	1.90	12.2
straight, fit	10.0	0.185	1.85	11.2

IV. CONCLUSIONS

In this paper, flapping wings with different leading edge shapes (curved or straight) and wing membrane tension (loosened or fit to the wing planform) were tested using a 1-DOF flapping mechanism based on measurement of a real hummingbird in hovering flight. It was found that the model wings composed of CFRP frames and a film membrane can realize feathering deformation similar to that of the real hummingbird in upstroke. In addition, we demonstrated that loosened wing membranes increase not only the wing area but also produce larger feathering deformation, resulting in enhancement of lift. Another suggestion is that curved shape of hummingbirds' leading edge also increases average lift. The wing with the curved leading edge and the loosened membrane generated the highest efficiency, calculated from input voltage and current, and the highest lift which is enough to support the weight of the hummingbird we measured. Our experiments imply that some portion of flight mechanism of hummingbird could be modeled as simple 1-DOF flapping with passive feathering deformation of the wing surface. In the future work, not only wing structure but also musculoskeletal biomechanism of the wings and flight muscles should be considered.

ACKNOWLEDGMENT

A part of this work is a cooperative research with Tama Zoological Park. The authors thank Kuniei Tabata and Chieko Fujii in the Tama Zoological Park for cooperative experiment of measurement of hummingbirds. We also thank Toshiyuki Nakata in The Royal Veterinary College, University of London for the development of the flapping mechanism.

REFERENCES

[1] S. P. Sane, "The aerodynamics of insect flight," *Journal of Experimental Biology,* vol. 206, pp. 4191-4208, Dec 2003.

[2] A. Azuma, *The Biokinetics of Flying and Swimming Second Edition*, 2 ed. Virginia: AIAA, 2006.

[3] S. S. Baek, F. L. G. Bermudez, and R. S. Fearing, "Flight control for target seeking by 13 gram ornithopter," in *Intelligent Robots and Systems (IROS), 2011 IEEE/RSJ International Conference on*, 2011, pp. 2674-2681.

[4] G. C. H. E. d. Croon, M. A. Groen, C. D. Wagter, B. Remes, R. Ruijsink, and B. W. v. Oudheusden, "Design, aerodynamics and autonomy of the DelFly," *Bioinspiration & Biomimetics,* vol. 7, p. 025003, 2012.

[5] T. Fujikawa, K. Hirakawa, S. Okuma, T. Udagawa, S. Nakano, and K. Kikuchi, "Development of a small flapping robot: Motion analysis during takeoff by numerical simulation and experiment," *Mechanical Systems and Signal Processing,* vol. 22, pp. 1304-1315, 2008.

[6] T. Nakata, H. Liu, Y. Tanaka, N. Nishihashi, X. Wang, and A. Sato, "Aerodynamics of a bio-inspired flexible flapping-wing micro air vehicle," *Bioinspiration & Biomimetics,* vol. 6, p. 045002, 2011.

[7] T. N. Pornsin-sirirak, Y. C. Tai, H. Nassef, and C. M. Ho, "Titanium-alloy MEMS wing technology for a micro aerial vehicle application," *Sensors and Actuators a-Physical,* vol. 89, pp. 95-103, Mar 2001.

[8] H. Tanaka and I. Shimoyama, "Forward flight of swallowtail butterfly with simple flapping motion," *Bioinspiration & Biomimetics,* vol. 5, p. 026003, 2010.

[9] N. O. Pérez-Arancibia, K. Y. Ma, K. C. Galloway, J. D. Greenberg, and R. J. Wood, "First controlled vertical flight of a biologically inspired microrobot," *Bioinspiration & Biomimetics,* vol. 6, p. 036009, 2011.

[10] H. Tanaka, J. P. Whitney, and R. J. Wood, "Effect of Flexural and Torsional Wing Flexibility on Lift Generation in Hoverfly Flight," *Integrative and Comparative Biology,* vol. 51, pp. 142-150, July 1, 2011 2011.

[11] M. Keennon, K. Klingebiel, H. Won, and A. Andriukov, "Developement of the Nano Hummingbird: A Tailless Flapping Wing Micro Air Vehicle," in *50th AIAA Aerospace Sciences Meeting including the New Horizons Forum and Aerospace Exposition*, Nashville, Tennessee, USA, 2012, pp. AIAA 20112-0588.

[12] P. Chai and D. Millard, "Flight and size constraints: Hovering performance of large hummingbirds under maximal loading," *Journal of Experimental Biology,* vol. 200, pp. 2757-2763, 1997.

[13] F. G. Stiles, D. L. Altshuler, and R. Dudley, "Wing morphology and flight behavior of some north American hummingbird species," *Auk,* vol. 122, pp. 872-886, 2005.

[14] D. L. Altshuler and R. Dudley, "The ecological and evolutionary interface of hummingbird flight physiology," *Journal of Experimental Biology,* vol. 205, pp. 2325-2336, 2002.

[15] T. L. Hedrick, B. W. Tobalske, I. G. Ros, D. R. Warrick, and A. A. Biewener, "Morphological and kinematic basis of the hummingbird flight stroke: scaling of flight muscle transmission ratio," *Proceedings of the Royal Society B: Biological Sciences,* vol. 279, pp. 1986-1992, May 22, 2012 2012.

[16] D. L. Altshuler, R. Dudley, and C. P. Ellington, "Aerodynamic forces of revolving hummingbird wings and wing models," *Journal of Zoology,* vol. 264, pp. 327-332, 2004.

[17] C. P. Ellington, "The aerodynamics of hovering insect flight III. Kinematics," *Philosophical Transactions of the Royal Society of London Series B-Biological Sciences,* vol. 305, pp. 41-78, 1984.

[18] B. W. Tobalske, D. R. Warrick, C. J. Clark, D. R. Powers, T. L. Hedrick, G. A. Hyder, *et al.*, "Three-dimensional kinematics of hummingbird flight," *J Exp Biol,* vol. 210, pp. 2368-2382, July 1, 2007 2007.

[19] D. R. Warrick, B. W. Tobalske, and D. R. Powers, "Aerodynamics of the hovering hummingbird," *Nature,* vol. 435, pp. 1094-1097, 2005.

[20] D. R. Warrick, B. W. Tobalske, and D. R. Powers, "Lift production in the hovering hummingbird," *Proceedings of the Royal Society B-Biological Sciences,* vol. 276, pp. 3747-3752, Nov 2009.